Inorganic Chemistry

pubs.acs.org/IC

Featured Article

Rational Design of Near-Infrared-Absorbing Pt(II)-Chelated Azadipyrromethene Dyes as a New Generation of Photosensitizers for Synergistic Phototherapy

Mingdang Li, Yunjian Xu, Menglong Zhao, Feiyang Li, Wei Feng, Teng Feng, Shujuan Liu,* and Qiang Zhao*

Cite This: https://dx.doi.org/10.1021/acs.inorgchem.0c02631

Read Online

ACCESS | Metrics & More | Article Recommendations | Supporting Information

ABSTRACT: Pt(II) photosensitizers are emerging as novel Pt anticancer agents for cancer photodynamic therapy (PDT) to avoid uncontrollable toxicity of cisplatin. However, the application of Pt(II) photosensitizers is limited by tumor hypoxia and the poor penetration depth of excitation light. To overcome these drawbacks, exploiting the next generation of Pt anticancer agents is of urgent need. According to theoretical calculations, novel near-infrared (NIR)-absorbing Pt(II)-chelated azadipyrromethene dyes (**PtDP-X**, where X = N, C, and S) were designed. Importantly, spin−orbit coupling of the Pt atom could promote the intersystem crossing of a singlet-to-triplet transition for converting oxygen to singlet oxygen ($^1O_2$), and the azadipyrromethene skeleton could provide a strong photothermal effect. As expected, **PtDP-X** exhibited intense NIR absorption and synergistic PDT and photothermal effects with low dark cytotoxicity. Furthermore, water-soluble and biocompatible **PtDP-N** nanoparticles (**PtDP-N NPs**) were prepared that achieved effective tumor cell elimination with low side effects under 730 nm light irradiation in vitro and in vivo. This pioneering work could push the exploitation of NIR-absorbing metal-chelated azadipyrromethene dyes, so as to promote the positive evolution of phototherapy agents.

INTRODUCTION

Platinum (Pt) anticancer drugs, such as cisplatin and its analogues, have long been utilized in the treatment of tumors. Cisplatin has been extensively used to treat testicular, ovarian, and bladder cancers, and the cure rates have significantly improved, demonstrating its remarkable clinical importance.[1,2] Despite their application in tumor treatment for over 40 years, cisplatin and its analogues have remained essential anticancer drugs.[3] However, ototoxicity, nephrotoxicity, and neurotoxicity of cisplatin always occur in the process of chemotherapy, which may lead to uncontrollable toxic side effects in cancer patients. Additionally, clinical issues pertaining to tumor resistance as well as limited pharmacokinetic properties further restrict these drugs from attaining their total efficacy.[4−6] In order to overcome these drawbacks, phototherapy has emerged as a noninvasive and controllable strategy for precise tumor ablation.[7,8] Photodynamic therapy (PDT), as an emerging phototherapy modality with low systemic toxicity and minimal invasiveness, has become an ideal platform for cancer therapy. During PDT, the photosensitizer that accumulated at the tumor location could transform the surrounding oxygen to cytotoxic singlet oxygen ($^1O_2$) upon irradiation with a certain wavelength of light, causing the destruction of organelles and leading to cancer cell death.[9−12] As a new type of Pt anticancer agent, Pt(II) photosensitizers have showcased promising potential in cancer phototherapy.[5,13−16] Many efforts have been made to improve the $^1O_2$ yield of Pt(II) photosensitizers to promote the therapeutic efficacy of tumor PDT. Although some reported Pt(II) photosensitizers exhibited good $^1O_2$ generation ability, the absorption located at the visible region still limited the penetration depth of the excitation light, restricting the reachable depth of PDT.[17−19] The poor penetration depth of conventional Pt(II) photosensitizers has become a serious barrier in treating deep-seated tumors. Consequently, expanding the absorption wavelength of Pt(II) photosensitizers to the near-infrared (NIR) range may serve as a breakthrough in increasing its penetration depth in biological tissues, although this would be a huge challenge. Fortunately, the chemical structure of a Pt(II) photosensitizer is easily modifiable. Thus, its rational design would provide significant opportunities in exploiting the next generation of Pt anticancer

Received: September 3, 2020

agents with the hope of realizing long-wavelength absorption and even multimode cancer phototherapy.[20,21]

To develop novel Pt(II)-based phototherapy agents with a deep PDT effect, the integration of Pt(II) ions and NIR organic dyes is a promising method.[22,23] In this regard, azadipyrromethene has been successfully used to develop the well-known NIR dye aza-BODIPYs by chelating with BF_2, which has often shown intense NIR absorption and high photostability in cancer photothermal therapy (PTT) since first being reported in 1943.[22,23] Considering the typical chelated moiety of N^NH in azadipyrromethene, a Pt(II) ion could directly replace the boron ion to acquire NIR-absorbing Pt(II)-chelated azadipyrromethene dyes.[24,25] Spin−orbit coupling of the Pt atom could promote the intersystem crossing of a singlet-to-triplet transition for converting oxygen to $^1O_2$. Accordingly, its direct chelation with azadipyrromethene could provide a PDT effect. Meanwhile, the azadipyrromethene skeleton could provide a strong photothermal effect. It is well-known that the hypoxic environment existing in the tumor region leads to a severely reduced anticancer efficacy of PDT. The photothermal effect of this dye is helpful in boosting blood flow in tumor regions and subsequently improving the oxygen concentration, so as to enhance the PDT efficacy.[26−29] Moreover, the PDT effect could eliminate the protective effect of heat shock protein 70 for tumor cells under photothermally induced heat stress.[30−32] Consequently, the complementary integration of PDT and PTT is achieved in one small-molecule dye, which is significant in developing synergistic therapy agents. Compared with other Pt-based synergistic phototherapy agents, the designed small-molecule dye could overcome complicated synthetic procedures and unbalanced integration of functional units.[33−35] In addition, the PDT effect and photothermal conversion efficiency of the designed dye could be easily adjusted by the modification of special functional groups to control their radiative or nonradiative transition.[36−38] As far as we know, the present study is the first to report the rational design of a NIR-absorbing Pt(II)-chelated azadipyrromethene dye for the evolution of Pt anticancer agents.

Under the guidance of time-dependent density functional theory (DFT) calculations, a novel series of NIR-absorbing Pt(II)-chelated azadipyrromethene dyes (**PtDP-X**, where X = N, C, and S) were successfully synthesized. As shown in Scheme 1a, dimethylamine-substituted azadipyrromethene was used as a skeleton for Pt(II) ion chelation to elongate the absorption wavelength. As expected, the absorption peak of **PtDP-X** was at about 700 nm, which was located at the biological spectral window (600−900 nm). Among **PtDP-X**, **PtDP-N** showed the best effects in PDT and PTT. In order to assess the anticancer performance of **PtDP-N** in vitro and in vivo, amphiphilic polymer DSPE-$mPEG_{5000}$ was used to encapsulate **PtDP-N** to acquire hydrophilic nanoparticles (**PtDP-N NPs**), so as to improve the water solubility, biocompatibility, and photostability. **PtDP-N NPs** possessed excellent synergistic PTT and PDT effects on both HeLa cells and HeLa tumor-bearing mice. Hence, the designed **PtDP-X** has shown great promise in becoming the next generation of Pt anticancer agents for tumor therapy. More than that, the ideas proposed in this study could be expanded into the rational design of NIR-absorbing metal-chelated azadipyrromethene dyes by changing the metal centers. The efforts made in this study may also provide a highly efficient and convenient solution for the positive evolution of phototherapy agents.

Scheme 1. (a) Chemical Structures of PtDP-N, PtDP-C, PtDP-S, BDP-N, BDP-C, and BDP-S, (b) Schematic Illustration of the Formation of PtDP-X NPs, and (c) Schematic Illustration of the Process of Tumor Ablation under a NIR Laser (730 nm) via Synergistic Phototherapy

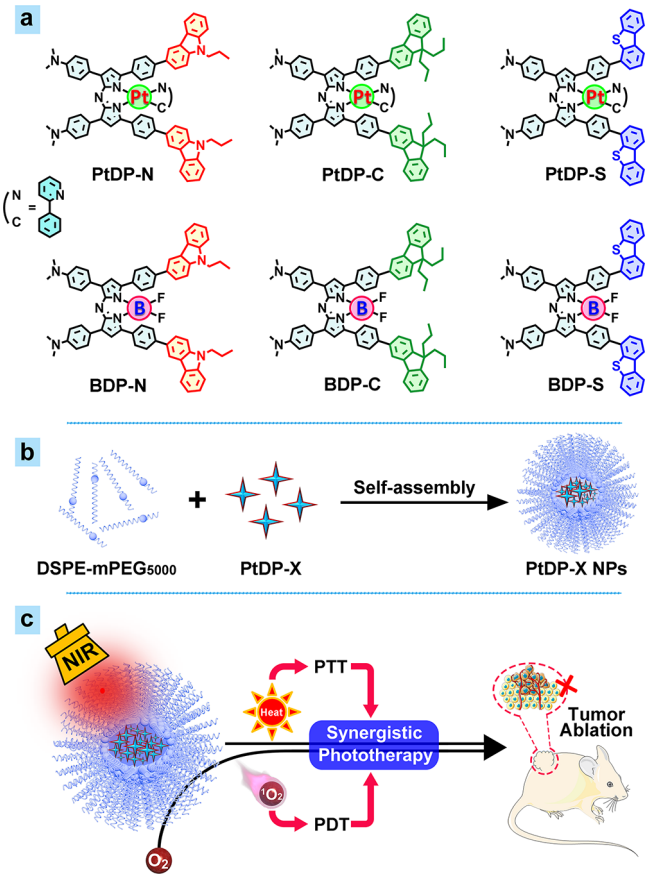

RESULTS AND DISCUSSION

DFT Calculation of PtDP-X. To exploit NIR-absorbing Pt(II)-chelated azadipyrromethene dyes, DFT was used to predict the photopysical properties of **PtDP-X**.[39,40] BF_2-chelated azadipyrromethenes (BDP-X; Scheme 1a) were calculated as control groups by replacing the Pt(II) ion of **PtDP-X** with BF_2. As shown in Table S1, the calculated absorption peaks of **PtDP-X** and BDP-X were all intense and at about 700 nm, which should be attributed to a $\pi-\pi^*$ transition of the azadipyrromethene skeleton. The energy-minimized calculated structures of **PtDP-X** and BDP-X were illustrated in Figures S1 and S2, respectively. There were obvious differences in the molecular orbitals of BDP-X and **PtDP-X**. The highest occupied molecular orbital (HOMO) of BDP-X was mainly located at the π orbital of the azadipyrromethene skeleton and *N*,*N*-dimethylaniline moieties, and the lowest unoccupied molecular orbital (LUMO) of BDP-X was mainly located at the π^* orbital of the N atom at the meso position of BDP-X and the azadipyrromethene skeleton with no electronic communications with the B atom, leading to the nonradiative transition for generating heat. The HOMO of **PtDP-X** was located on the $d_{x^2-y^2}$ orbital of the Pt atom and the π orbital of the azadipyrromethene skeleton and *N*,*N*-dimethylaniline moieties. The LUMO of **PtDP-X** was mainly located on the π^* orbital of the azadipyrromethene skeleton. The $\pi-\pi^*$ transition could allow nonradiative decay for producing heat.

https://dx.doi.org/10.1021/acs.inorgchem.0c02631
Inorg. Chem. XXXX, XXX, XXX−XXX

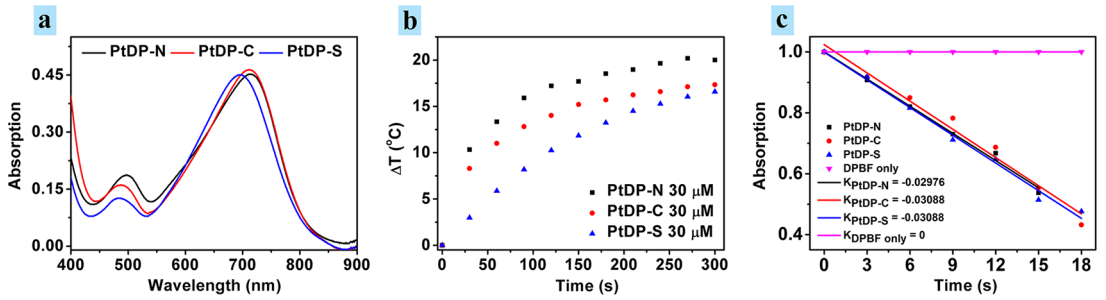

Figure 1. (a) Absorption spectra of **PtDP-X** (X = N, C, and S) in THF. (b) Temperature elevation of **PtDP-X** (X = N, C, and S; 30 μM) in DMF (5% THF). (c) Absorption of DPBF in the solution of **PtDP-X** at 414 nm versus irradiation time (690 nm laser irradiation 500 mW cm^{-2}).

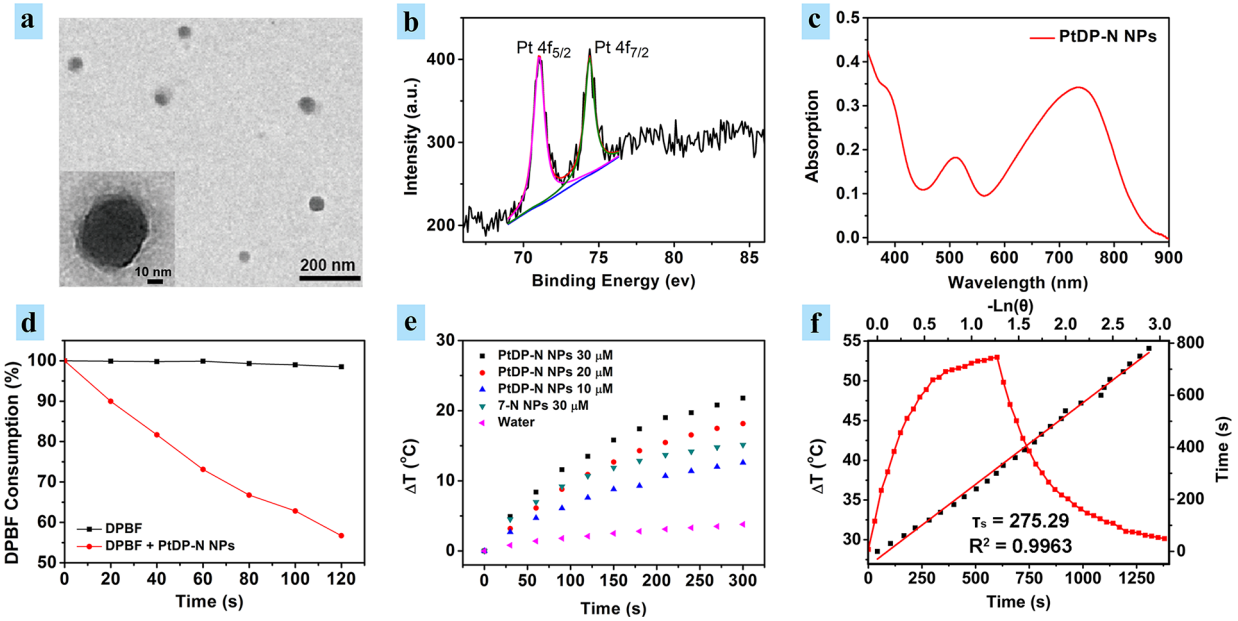

Figure 2. (a) TEM image of **PtDP-N NPs** (bar = 200 nm). The inset is the enlarged TEM image of **PtDP-N NPs** (bar = 10 nm). (b) XPS pattern of **PtDP-N NPs**. (c) Absorption spectra of **PtDP-N NPs** in water. (d) Absorption of DPBF in a solution of **PtDP-N NPs** (60 μM) and DPBF only at 414 nm versus irradiation time (730 nm laser irradiation; 500 mW cm^{-2}). (e) Temperature elevation of **PtDP-N NPs** at different concentrations and **7-N NPs** (30 μM) under a 730 nm laser (500 mW cm^{-2}) irradiation. (f) Photothermal conversion efficiency calculation of **PtDP-N NPs** (30 μM) under a 730 nm laser (500 mW cm^{-2}) irradiation.

The metal-to-ligand charge transfer between the Pt atom and azadipyrromethene skeleton could allow the radiative transition. However, the large spin−orbit coupling of the Pt atom could promote the intersystem crossing of a singlet-to-triplet transition, which is able to convert oxygen to $^1O_2$. Hence, we predict that **PtDP-X** would possess PDT and PTT effects simultaneously.

Synthesis and Characterization of PtDP-X. In this study, the designed **PtDP-X** (X = N, C, and S) was successfully synthesized through a facile and feasible approach. There are two main steps: (i) a series of azadipyrromethene derivatives functionalized with carbazole, fluorene, and benzothiophene, respectively, were synthesized as the ligands; (ii) under an atmosphere of N_2, the ligands, together with 0.5 equiv of Pt(II) chloro-bridged dimers and 5 equiv of Na_2CO_3, were refluxed at 110 °C in 2-ethoxyethanol for 4 h. BDP-X were synthesized as control groups. The details of the synthetic procedures are shown in Scheme S1. The chemical structures of all compounds were characterized by ^{1}H NMR and matrix-assisted laser desorption/ionization time-of-flight mass spectrometry.

Photophysical Properties of PtDP-X. The photophysical properties of **PtDP-X** in tetrahydrofuran (THF) solution were summarized in Table S2. As shown in Figure 1a, the NIR absorption peaks of **PtDP-N**, **PtDP-C**, and **PtDP-S** were at 717, 710, and 693 nm, respectively. Besides, compared with **PtDP-C** and **PtDP-S**, the maximal absorption peak of **PtDP-N** was red-shifted because of the stronger electron-donating ability of carbazole than that of fluorene and benzothiophene. Their molar absorption coefficients at the maximum peaks were 0.500 × 10^5, 0.464 × 10^5, and 0.450 × 10^5 M^{-1} cm^{-1}, respectively. As summarized in Table S2, the emission peaks with maximum intensity were at 811, 810, and 807 nm for **PtDP-N**, **PtDP-C**, and **PtDP-S**, respectively. Compared with BDP-X, **PtDP-X** showed lower fluorescence quantum yields, indicating that chelation of the Pt atom could promote the intersystem crossing of a singlet-to-triplet transition, and the triplet state of **PtDP-X** could relax to the ground state via nonradiative decay. In this nonradiative decay process, the triplet-state energy of **PtDP-X** could be transferred to oxygen to produce $^1O_2$.

Photothermal and Photodynamic Properties of PtDP-X. Considering that **PtDP-X** exhibited similar absorption

https://dx.doi.org/10.1021/acs.inorgchem.0c02631
Inorg. Chem. XXXX, XXX, XXX−XXX

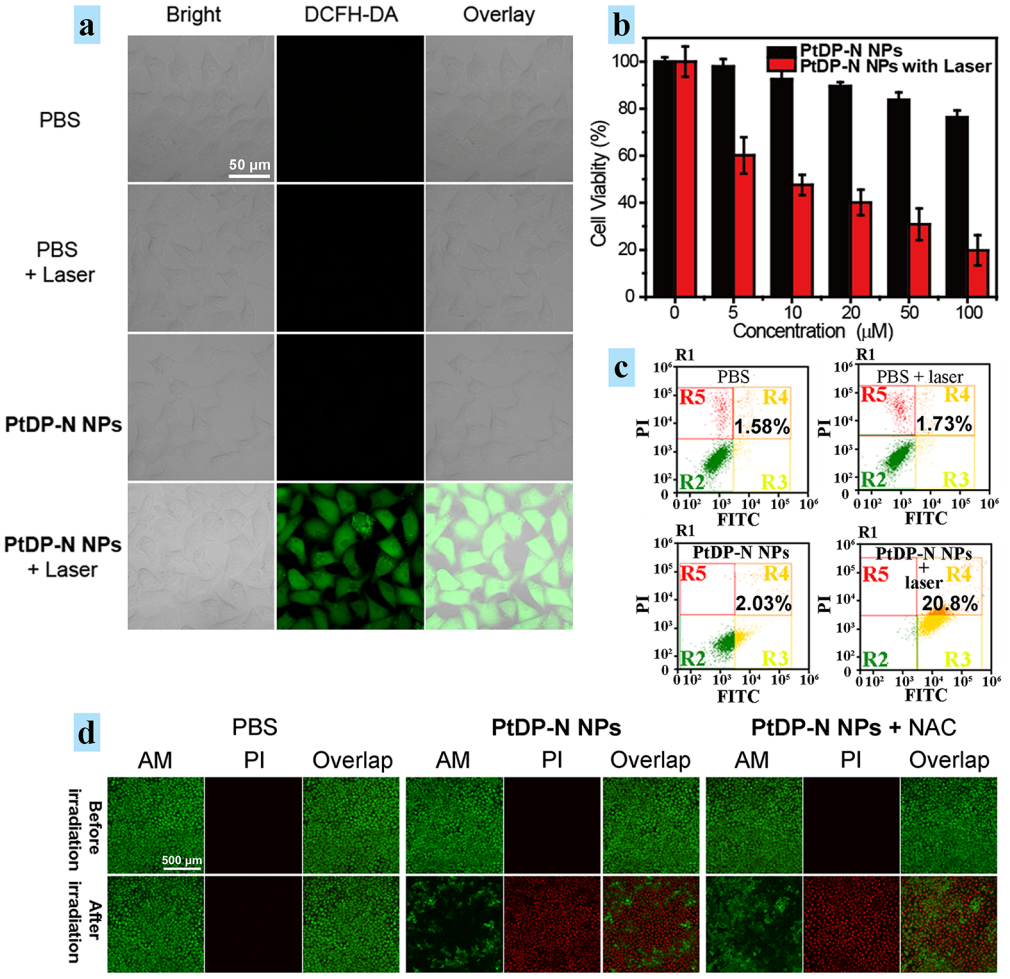

Figure 3. (a) Confocal fluorescence images of $^1O_2$ generation in HeLa cells (bar = 50 μm). (b) Relative viability of HeLa cells treated with **PtDP-N NPs** at various doses at 24 h after 5 min of 730 nm laser (500 mW cm^{-2}) irradiation. (c) Flow cytometry of HeLa cells treated with **PtDP-N NPs** at the dose of 20 μM for 12 h of incubation under 5 min of irradiation or not (730 nm, 500 mW cm^{-2}) using an Annexin V-FITC/PI apoptosis detection kit. (d) Confocal fluorescence images of HeLa cells (cultured with PBS, **PtDP-N NPs**, and **PtDP-N NPs** + NAC) before and after irradiation, which were stained by both Calcein AM and PI (bar = 500 μm).

abilities at 690 nm, we evaluated their photothermal properties with a 690 nm laser (500 mW cm^{-2}). The **PtDP-X** solution in *N*,*N*-dimethylformamide (DMF; 5% THF) was prepared in different concentrations (10, 20, and 30 μM). All of them were irradiated with the above selected laser for 5 min. Their temperature changes were recorded by a thermal infrared imager (FLIR E40). As shown in Figures 1b and S3a,b, **PtDP-N** exhibited the highest temperature change at every concentration. Especially, the temperature change of **PtDP-N** was 20.0 °C at 30 μM, which was 2.7 and 3.4 °C higher than those of **PtDP-C** and **PtDP-S**, respectively, demonstrating that **PtDP-N** possessed the most excellent photothermal effect among **PtDP-X**. Also, the slight temperature change of a blank DMF (5% THF) solution indicated that the solvent had no influence on the photothermal effect of **PtDP-X** (Figure S3c). Importantly, the temperature change of **PtDP-N** at 30 μM was similar to that of BDP-N (Figure S3d), which further indicated the good photothermal effect of **PtDP-N**.

The PDT effect of **PtDP-X** was evaluated by the reactive oxygen species (ROS) indicator diphenylisobenzofuran (DPBF).[41] As shown in Figures 1c and S4, the 414 nm absorption peak of the DPBF solution showed a negligible decrease when it was irradiated by a 690 nm laser (500 mW cm^{-2}). Also, the absorption peak at 414 nm of mixed solutions of DPBF and **PtDP-X** decreased dramatically, which confirmed its good ROS generation ability. The result indicated that **PtDP-X** can be applied as a good PDT agent. The PDT effect of **PtDP-X** under the same conditions was similar, demonstrating that the substituent groups (carbazole, fluorene, and benzothiophene) of **PtDP-X** cannot influence their PDT effect. In addition, the 414 nm absorption peak of a mixed DPBF and BDP-N solution did not change, which demonstrated that the ROS cannot be generated from the excited state of BDP-N because of the absence of a heavy-atom effect. The results presumably indicated that the heavy atom Pt with a large spin−orbit coupling constant could promote the intersystem crossing of a singlet-to-triplet transition for increasing the $^1O_2$ generation ability. In this work, NIR-absorbing **PtDP-N** with the best PTT effect and a good PDT effect was selected as the phototherapy agent to perform the following experiments.

Preparation and Characterization of PtDP-N NPs. In order to improve the water solubility, biocompatibility, and photostability of **PtDP-N**, the amphiphilic polymer DSPE-mPEG$_{5000}$ was used to encapsulate **PtDP-N** to acquire hydrophilic nanoparticles (**PtDP-N NPs**), and the obtained

https://dx.doi.org/10.1021/acs.inorgchem.0c02631
Inorg. Chem. XXXX, XXX, XXX−XXX

PtDP-N NPs could disperse in water uniformly. The loading content of **PtDP-N NPs** was calculated by the standard curve method (Figure S5). The details of the synthetic procedures and test methods are shown in the Supporting Information. As shown in Figure 2a, **PtDP-N NPs** have uniform sizes with diameters of around 50 nm, which were measured by transmission electron microscopy (TEM). As shown in Figure S7, the hydrodynamic size measured by dynamic light scattering was 92 nm, which was very suitable for bioapplication. Also, the hydrodynamic size changed negligibly at 72 h, indicating the excellent stability of **PtDP-N NPs** in water. In addition, the energy-dispersive X-ray spectrum of **PtDP-N NPs** verifies the presence of the Pt atom (Figure S8). The presence of Pt(II) ions in the obtained nanoparticles was further confirmed by X-ray photoelectron spectroscopy (XPS). As shown in Figure 2b, there were two peaks at 71.1 and 74.5 eV, indicating the existence of Pt(4f) in **PtDP-N NPs**. In addition, the maximal absorption peak of **PtDP-N NPs** was at 732 nm. As shown in Figure 2c, the absorption band of **PtDP-N NPs** in the NIR region was broadened and red-shifted compared with free **PtDP-N**, which was caused by $\pi-\pi$ stacking of **PtDP-N** in the micellar cores. As shown in Figure S9, the **PtDP-N NPs** aqueous solution showed weak luminescence because of their low luminescent quantum efficiencies and aggregation-induced quenching.

Photothermal and Photodynamic Properties of PtDP-N NPs. At first, the photothermal effect of **PtDP-N NPs** was investigated. The temperature changes of the **PtDP-N NPs** aqueous solution with different concentrations were measured under continuous irradiation of a 730 nm laser (500 mW cm^{-2}) for 5 min. As shown in Figure 2e, a quick elevation of the temperature was observed in the **PtDP-N NPs** solution at every concentration, while the temperature of pure water showed no obvious change. On the basis of the data in Figure 2f and the reported method,[42−46] the photothermal conversion efficiency of **PtDP-N NPs** was calculated as 27.9%. This value is significantly higher than that of commercial dye ICG (15.1%), which has been approved by the Federal Drug Administration for NIR photothermal agents.[47] Importantly, the temperature change of azadipyrromethene nanoparticles (**7-N NPs**) at 30 μM was 15.7 °C (Figure 2e). The results confirmed that the photothermal effect of **PtDP-N** was produced by the azadipyrromethene skeleton. Furthermore, to assess the photothermal stability of **PtDP-N NPs**, a thermocycling test was performed. As shown in Figure S10, **PtDP-N NPs** exhibited a negligible temperature change after five repeated cycles, suggesting the excellent photothermal stability of **PtDP-N NPs**. Hence, **PtDP-N** still retained excellent photothermal effect and stability after being encapsulated in **PtDP-N NPs**.

Next, the photostability test of **PtDP-N NPs** was carried out by monitoring the maximal absorption under long-time irradiation of a 730 nm laser. As shown in Figure S11, the intensity of the maximal absorption peak of **PtDP-N NPs** exhibited almost no change even under irradiation for 30 min, suggesting the excellent photostability of **PtDP-N NPs**. The $^1O_2$ generation of **PtDP-N NPs** was confirmed by monitoring the 414 nm absorption changes of DPBF, when the mixed DPBF, superoxide dismutase, catalase, and **PtDP-N NPs** solution was irradiated by a 730 nm laser (500 mW cm^{-2}). As shown in Figures 2d and S12, the absorption intensity of DPBF decreased about 40% after 2 min of irradiation. In contrast, a slight decrease was observed in the DPBF-only group. The results demonstrated that the **PtDP-N NPs** have good $^1O_2$ generation ability for realizing a PDT effect.

In Vitro Photothermal and Photodynamic Properties of PtDP-N NPs. With the purpose of exploring the biomedical applications of **PtDP-N NPs**, their PDT and PTT effects were detected in vitro. First, 2′,7′-dichlorofluorescin diacetate (DCFH-DA, a ROS indicator) was used to detect ROS generation of **PtDP-N NPs** in HeLa cells.[48] As shown in Figure 3a, the green fluorescence was observed in **PtDP-N NPs**-treated cells after 5 min of light irradiation (730 nm, 500 mW cm^{-2}), while no or weak fluorescence could be seen in the control groups. The result confirmed the effective ROS generation ability of **PtDP-N NPs** in HeLa cells. Next, the cytotoxicity of **PtDP-N NPs** was investigated by MTT assays. The HeLa cells were incubated with **PtDP-N NPs** at a series of concentrations. The pretreated cells were irradiated with 730 nm light (500 mW cm^{-2}) for 5 min or not to measure the light or dark cytotoxicity of **PtDP-N NPs**. As shown in Figure 3b, the viability of HeLa cells was more than 80% in the dark even with concentrations of up to 100 μM, which indicated low dark cytotoxicity and excellent biocompatibility. Under irradiation, the viability of **PtDP-N NPs**-treated HeLa cells sharply decreased with increasing **PtDP-N NPs** concentration. When the concentration of **PtDP-N NPs** was 20 μM, the viability of HeLa cells was about 50% of the original value. The results demonstrated that **PtDP-N NPs** have a good phototherapy effect for effectively killing cancer cells. In order to further illustrate the phototherapy effect of **PtDP-N NPs** to cause cell apoptosis and cell death, flow cytometry experiments were completed via an Annexin V-FITC/propidium iodide (PI) cell apoptosis kit to ensure the amounts of viable and dead cells of different stages with the given conditions. As shown in Figure 3c, few HeLa cells were at the late apoptotic stage in the groups of phosphate-buffered saline (PBS) only, PBS with a laser, and **PtDP-N NPs** only. However, 20.8% HeLa cells at the late apoptotic stage were detected when they were incubated with **PtDP-N NPs** and treated with a laser. Hence, **PtDP-N NPs** with an excellent phototherapy effect could effectively inhibit the growth of cancer cells.

To evaluate the synergistic PDT and PTT effects of **PtDP-N NPs**, a live−dead cell staining experiment was applied to HeLa cells. The green fluorescence of Calcein AM and red fluorescence of PI expressed live and dead cells, respectively. *N*-Acetyl-L-cysteine (NAC) could react with ROS to inhibit the PDT effect of **PtDP-N NPs** and leave the PTT effect only. To rule out the fluorescence interference of **PtDP-N NPs**, confocal fluorescence (**PtDP-N NPs** without AM, PI, and HeLa cells) in green and red channels was performed. As shown in Figure S13, no fluorescence was observed under 488 nm laser irradiation, indicating that **PtDP-N NPs** cannot affect this test. As shown in Figure 3d, there was only green fluorescence before laser irradiation in every group. However, intense red fluorescence was observed in the **PtDP-N NPs** and **PtDP-N NPs** + NAC groups. Also, the intensity of the green fluorescence in the **PtDP-N NPs** group was obviously weaker than that of the **PtDP-N NPs** + NAC group. The results demonstrated that **PtDP-N NPs** exhibited good synergistic PDT and PTT effects for killing cancer cells.

In Vivo Photothermal and Photodynamic Properties of PtDP-N NPs. Considering the good synergistic PDT and PTT effects of **PtDP-N NPs** in cells, the phototherapy effect on HeLa tumor-bearing mice was further investigated. All animal experiments conformed to the National Institutes of

https://dx.doi.org/10.1021/acs.inorgchem.0c02631
Inorg. Chem. XXXX, XXX, XXX−XXX

Health guidelines for care and use. Generally, local temperatures higher than 43 °C will harm tumors.[18] As shown in Figures 4a and S14, the temperature of the tumor sites injected

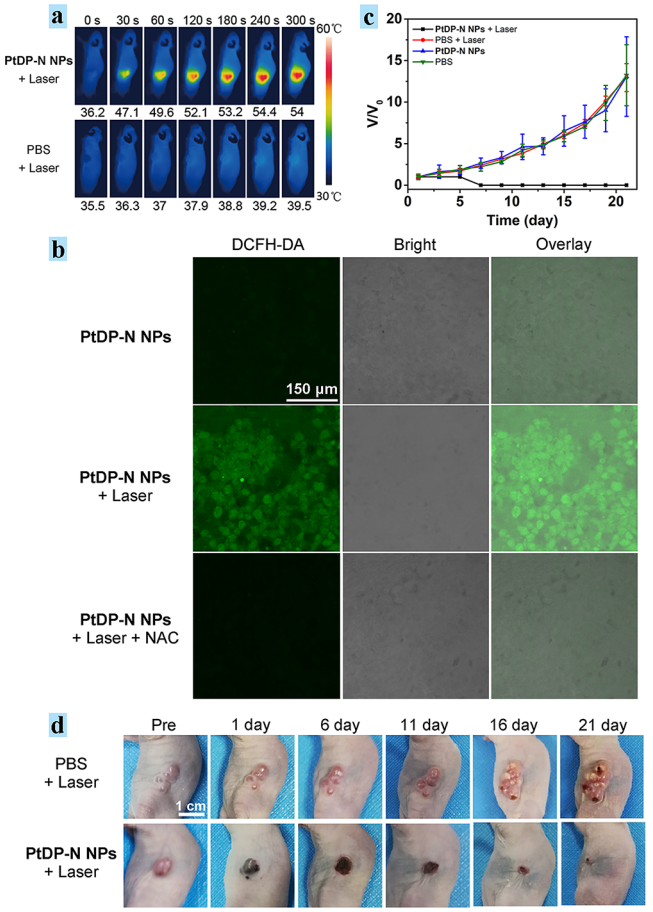

Figure 4. (a) IR thermal images of a mouse injected with a **PtDP-N NPs** solution and a mouse injected with a PBS solution under 730 nm irradiation (500 mW cm^{-2}) for 5 min. (b) Confocal fluorescence images of DCFH-DA-stained tumor sections (bar = 150 μm). (c) Relative tumor volume for different groups of mice (n = 3). (d) Images of tumor-bearing mice at various time points after treatment (**PtDP-N NPs** with a laser group and PBS with a laser group).

with **PtDP-N NPs** increased rapidly with prolongation of the irradiation time. After 5 min of laser irradiation, the temperature of the tumor sites increased up to 54 °C, which could effectively eliminate tumors. In the control groups, the temperature of the tumor sites without **PtDP-N NPs** elevated to only 39.5 °C even after 5 min of laser irradiation, which does no harm to cells. The results indicated the excellent PTT effect of **PtDP-N NPs** in vivo.

In addition, DCFH-DA was used to detect the ROS generation of **PtDP-N NPs** in tumor parts. The mice treated with **PtDP-N NPs**, DCFH-DA, and a laser acted as experimental groups. **PtDP-N NPs**- and DCFH-DA-treated mice acted as control groups, while **PtDP-N NPs**-, DCFH-DA-, NAC-, and laser-treated mice were used as additional control groups. After 5 min of laser irradiation or not, tumors were sliced and observed by a confocal laser scanning microscope. As shown in Figure 4b, no fluorescence was observed in all control groups. In contrast, the green fluorescence was intense in the experimental groups. The results indicated that **PtDP-N NPs** have effective ROS generation ability and confirmed that they could possess a PDT effect in vivo.

In Vivo Synergistic Phototherapy of PtDP-N NPs. Inspired by both the PDT and PTT effects of **PtDP-N NPs** in tumors, a synergistic phototherapy experiment was carried out on HeLa tumor-bearing mice. When the volume of the tumors reached about 100 mm^3, the HeLa tumor-bearing mice were divided into four groups, namely, PBS only, PBS with a laser (730 nm, 500 mW cm^{-2}), **PtDP-N NPs** only, and **PtDP-N NPs** with a laser (730 nm, 500 mW cm^{-2}). The mice treated with **PtDP-N NPs** and a laser acted as the experimental groups, while the remaining mice acted as the control group. Furthermore, the synergistic PDT and PTT effects of **PtDP-N NPs** in vivo were monitored by recording the change of the tumor volume every day. As shown in Figure 4c,d, the tumors became larger with the extension of time in the control groups, and the volume of these tumors was about 13 times bigger than that of the initial tumors after 21 days of care. In contrast, the tumor volumes of mice in the experimental group disappeared completely, with black scars after 6 days (5 min of laser irradiation three times every 2 days) of phototherapy. Then the phototherapy was stopped. The scars almost dropped until 21 days later. The mice were dissected and no tumor was found, indicating the excellent synergistic PDT and PTT effects of **PtDP-N NPs**. Besides, the body weight of the mouse is a very important index to evaluate the efficiency of tumor phototherapy. The body weights of all mice in various groups exhibited negligible fluctuation, indicating the low toxicity of **PtDP-N NPs** (Figures S15 and S16). All of the results collectively confirmed that **PtDP-N NPs** could effectively eliminate the tumor in vivo with low side effects through the synergistic PDT and PTT effects under a single NIR laser irradiation.

To evaluate the possible toxicity of **PtDP-N NPs** in vivo, hematoxylin and eosin (H&E) staining of the tumors was completed to investigate their pathomorphology for one mouse of each group after 20 days of treatment. As shown in Figure S17, no obvious malignant necrosis was detected in the control groups, while the tumors were completely regressed in the experimental groups. Meanwhile, major organs (heart, liver, spleen, lung, muscle, and kidneys) were harvested from the control nd experimental groups after 20 days of treatment. As shown in Figure S18, H&E staining of the major organs from the experimental groups showed no obvious pathological change compared with those from the control groups. These results clearly demonstrated the negligible toxicity of **PtDP-N NPs** in vivo. Therefore, the biocompatible **PtDP-N NPs** with synergistic PDT and PTT effects were promising for using in clinical tumor-related phototherapy.

CONCLUSION

In this work, a new generation of Pt phototherapy agents, namely, NIR-absorbing Pt-chelated azadipyrromethene dyes, were successfully designed and synthesized. The absorption wavelength of these dyes was extended from the visible region to the biological spectral window (600−900 nm), which would effectively increase the reachable depth of PDT. Compared with traditional aza-BODIPY dyes, the designed dyes showed synergistic PDT and PTT effects. Furthermore, water-soluble and biocompatible phototherapy agents based on these dyes could achieve effective elimination of tumor cells with low side effects through synergistic PDT and PTT under a single NIR wavelength laser (730 nm, 500 mW cm^{-2}) in vitro and in vivo.

https://dx.doi.org/10.1021/acs.inorgchem.0c02631
Inorg. Chem. XXXX, XXX, XXX−XXX

Therefore, these dyes have promising potential for clinical tumor-related applications. More importantly, on the basis of the design strategy and synthetic methods proposed in this work, the exploitation of other NIR-absorbing metal-chelated azadipyrromethene dyes can be anticipated, which is underway in our laboratory.

■ ASSOCIATED CONTENT

Supporting Information

The Supporting Information is available free of charge at https://pubs.acs.org/doi/10.1021/acs.inorgchem.0c02631.

Synthesis, characterization, experimental information, additional figures and table, and author contributions (PDF)

■ AUTHOR INFORMATION

Corresponding Authors

Shujuan Liu − *Key Laboratory for Organic Electronics and Information Displays and Jiangsu Key Laboratory for Biosensors, Institute of Advanced Materials, Nanjing University of Posts and Telecommunications, Nanjing 210023, P. R. China*; Email: iamsjliu@njupt.edu.cn

Qiang Zhao − *Key Laboratory for Organic Electronics and Information Displays and Jiangsu Key Laboratory for Biosensors, Institute of Advanced Materials, Nanjing University of Posts and Telecommunications, Nanjing 210023, P. R. China*; orcid.org/0000-0002-3788-4757; Email: iamqzhao@njupt.edu.cn

Authors

Mingdang Li − *Key Laboratory for Organic Electronics and Information Displays and Jiangsu Key Laboratory for Biosensors, Institute of Advanced Materials, Nanjing University of Posts and Telecommunications, Nanjing 210023, P. R. China*

Yunjian Xu − *Key Laboratory for Organic Electronics and Information Displays and Jiangsu Key Laboratory for Biosensors, Institute of Advanced Materials, Nanjing University of Posts and Telecommunications, Nanjing 210023, P. R. China*

Menglong Zhao − *Key Laboratory for Organic Electronics and Information Displays and Jiangsu Key Laboratory for Biosensors, Institute of Advanced Materials, Nanjing University of Posts and Telecommunications, Nanjing 210023, P. R. China*

Feiyang Li − *Key Laboratory for Organic Electronics and Information Displays and Jiangsu Key Laboratory for Biosensors, Institute of Advanced Materials, Nanjing University of Posts and Telecommunications, Nanjing 210023, P. R. China*

Wei Feng − *Key Laboratory for Organic Electronics and Information Displays and Jiangsu Key Laboratory for Biosensors, Institute of Advanced Materials, Nanjing University of Posts and Telecommunications, Nanjing 210023, P. R. China*

Teng Feng − *Key Laboratory for Organic Electronics and Information Displays and Jiangsu Key Laboratory for Biosensors, Institute of Advanced Materials, Nanjing University of Posts and Telecommunications, Nanjing 210023, P. R. China*

Complete contact information is available at: https://pubs.acs.org/10.1021/acs.inorgchem.0c02631

Notes

The authors declare no competing financial interest.

■ ACKNOWLEDGMENTS

The authors acknowledge financial support from the National Funds for Distinguished Young Scientists (Grant 61825503), National Natural Science Foundation of China (Grants 61775101 and 61805122), National Key Research and Development Program of China (Grant 2017YFA0205302), and Open Research Fund of State Key Laboratory of Bioelectronics, Southeast University.

■ REFERENCES

(1) Abu-Surrah, A. S.; Kettunen, M. Platinum group antitumor chemistry: design and development of new anticancer drugs complementary to cisplatin. *Curr. Med. Chem.* **2006**, *13* (11), 1337−1357.

(2) Takahara, P. M.; Rosenzweig, A. C.; Frederick, C. A.; Lippard, S. J. Crystal structure of double-stranded DNA containing the major adduct of the anticancer drug cisplatin. *Nature* **1995**, *377*, 649−652.

(3) Rosenberg, B.; Vancamp, L.; Trosko, J. E.; Mansour, V. H. Platinum compounds: a class of potent antitumour agents. *Nature* **1969**, *222* (26), 385−386.

(4) Rabik, C. A.; Dolan, M. E. Molecular mechanisms of resistance and toxicity associated with platinating agents. *Cancer Treat. Rev.* **2007**, *33* (1), 9−23.

(5) Xue, X. L.; Qian, C. G.; Fang, H. B.; Liu, H. K.; Yuan, H.; Guo, Z. J.; Bai, Y.; He, W. J. Photoactivated lysosomal escape of monofunctional Pt(II) complex Pt-BDPA for nucleus access. *Angew. Chem., Int. Ed.* **2019**, *58* (36), 12661−12666.

(6) Samimi, G.; Kishimoto, S.; Manorek, G.; Breaux, J. K.; Howell, S. B. Novel mechanisms of platinum drug resistance identified in cells selected for resistance to JM118 the active metabolite of satraplatin. *Cancer Chemother. Pharmacol.* **2006**, *59*, 301−312.

(7) Yu, Y. J.; Xu, Q.; He, S. S.; Xiong, H. J.; Zhang, Q. F.; Xu, W. G.; Ricotta, V.; Bai, L.; Zhang, Q.; Yu, Z. Q.; Ding, J. X.; Xiao, H. H.; Zhou, D. F. Recent advances in delivery of photosensitive metal-based drugs. *Coord. Chem. Rev.* **2019**, *387*, 154−179.

(8) Xie, Z. J.; Fan, T. J.; An, J. S.; Choi, W.; Duo, Y. H.; Ge, Y. Q.; Zhang, B.; Nie, G. H.; Xie, N.; Zheng, T. T.; Chen, Y.; Zhang, H.; Kim, J. S. Emerging combination strategies with phototherapy in cancer nanomedicine. *Chem. Soc. Rev.* **2020**, *49*, 8065.

(9) Lv, W.; Zhang, Z.; Zhang, K. Y.; Yang, H. R.; Liu, S. J.; Xu, A. Q.; Guo, S.; Zhao, Q.; Huang, W. A mitochondria-targeted photosensitizer showing improved photodynamic therapy effects under hypoxia. *Angew. Chem., Int. Ed.* **2016**, *55* (34), 9947.

(10) Lo, P. C.; Rodríguez-Morgade, M. S.; Pandey, R. K.; Ng, D. K. P.; Torres, T.; Dumoulin, F. The unique features and promises of phthalocyanines as advanced photosensitisers for photodynamic therapy of cancer. *Chem. Soc. Rev.* **2020**, *49* (4), 1041−1056.

(11) Xiu, W. J.; Gan, S. Y.; Wen, Q. R.; Qiu, Q.; Dai, S. L.; Dong, H.; Li, Q.; Yuwen, L. H.; Weng, L. X.; Teng, Z. G.; Mou, Y. B.; Wang, L. H. Biofilm microenvironment-responsive nanotheranostics for dual-mode imaging and hypoxia-relief-enhanced photodynamic therapy of bacterial infections. *Research* **2020**, *2020*, 1.

(12) Qi, S. J.; Kwon, N.; Yim, Y.; Nguyen, V. N.; Yoon, J. Fine-tuning the electronic structure of heavy-atom-free BODIPY photosensitizers for fluorescence imaging and mitochondria-targeted photodynamic therapy. *Chem. Sci.* **2020**, *11* (25), 6479−6484.

(13) Guo, Z. Q.; Zou, Y. L.; He, H.; Rao, J. M.; Ji, S. S.; Cui, X. N.; Ke, H. T.; Deng, Y. B.; Yang, H.; Chen, C. Y.; Zhao, Y. L.; Chen, H. B. Bifunctional platinated nanoparticles for photoinduced tumor ablation. *Adv. Mater.* **2016**, *28* (46), 10155−10164.

(14) Lv, Z.; Zou, L.; Wei, H. J.; Liu, S. J.; Huang, W.; Zhao, Q. Phosphorescent starburst Pt(II) porphyrins as bifunctional therapeutic agents for tumor hypoxia imaging and photodynamic therapy. *ACS Appl. Mater. Interfaces* **2018**, *10* (23), 19523−19533.

(15) Ponte, F.; Alberto, M. E.; De Simone, B. C.; Russo, N.; Sicilia, E. Photophysical exploration of dual-approach Pt^{II}-BODIPY conjugates: theoretical insights. *Inorg. Chem.* **2019**, *58* (15), 9882−9889.
(16) Ramu, V.; Gautam, S.; Garai, A.; Kondaiah, P.; Chakravarty, A. R. Glucose-appended platinum(II)-BODIPY conjugates for targeted photodynamic therapy in red light. *Inorg. Chem.* **2018**, *57* (4), 1717−1726.
(17) Fan, W. P.; Huang, P.; Chen, X. Y. Overcoming the Achilles' heel of photodynamic therapy. *Chem. Soc. Rev.* **2016**, *45* (23), 6488−6519.
(18) Li, X. S.; Kwon, N.; Guo, T.; Liu, Z.; Yoon, J. Y. Innovative strategies for hypoxic-tumor photodynamic therapy. *Angew. Chem., Int. Ed.* **2018**, *57* (36), 11522−11531.
(19) Fan, W. P.; Bu, W. B.; Shi, J. L. On the latest three-stage development of nanomedicines based on upconversion nanoparticles. *Adv. Mater.* **2016**, *28* (21), 3987−4011.
(20) Kalinowski, J.; Fattori, V.; Cocchi, M.; Williams, J. A. G. Light-emitting devices based on organometallic platinum complexes as emitters. *Coord. Chem. Rev.* **2011**, *255*, 2401−2425.
(21) Naik, A.; Rubbiani, R.; Gasser, G.; Spingler, B. Visible-light-induced annihilation of tumor cells with platinum-porphyrin conjugates. *Angew. Chem., Int. Ed.* **2014**, *53* (27), 6938−6941.
(22) Rogers, M. Synthesis of 2:4-diarylpyrroles and 2:2′:4:4′-tetraarylaxadipyrrornethine. *J. Chem. Soc.* **1943**, *158*, 590−596.
(23) Xu, Y. J.; Feng, T.; Yang, T. S.; Wei, H. J.; Yang, H. R.; Li, G.; Zhao, M. L.; Liu, S. J.; Huang, W.; Zhao, Q. Utilizing intramolecular photoinduced e Electron transfer to enhance photothermal tumor treatment of aza-BODIPY-based near-infrared nanoparticles. *ACS Appl. Mater. Interfaces* **2018**, *10* (19), 16299−16307.
(24) Deligonul, N.; Gray, T. G. Azadipyrromethene complexes of d^8 metal centers: Rhodium(I), Iridium(I), Palladium(II), and Platinum-(II). *Inorg. Chem.* **2013**, *52* (22), 13048−13057.
(25) Williams, J. A. G.; Develay, S.; Rochester, D. L.; Murphy, L. Optimising the luminescence of platinum(II) complexes and their application in organic light emitting devices (OLEDs). *Coord. Chem. Rev.* **2008**, *252* (23−24), 2596−2611.
(26) Zhao, M. L.; Xie, M. J.; Guo, J. G.; Feng, W.; Xu, Y. J.; Liu, X. M.; Liu, S. J.; Zhao, Q. Facile phototherapeutic nanoplatform by integrating a multifunctional polymer and MnO_2 for enhancing tumor synergistic therapy. *Adv. Healthcare Mater.* **2019**, *8* (7), 1900414.
(27) Tang, Q. Y.; Si, W. L.; Huang, C. H.; Ding, K. K.; Huang, W.; Chen, P.; Zhang, Q.; Dong, X. C. Aza-Bodipy photosensitizer for photoacoustic and photothermal imaging guided dual modal cancer phototherapy. *J. Mater. Chem. B* **2017**, *5* (8), 1566−1573.
(28) Miao, W.; Kim, H.; Gujrati, V.; Kim, J.; Jon, H.; et al. Photo-decomposable organic nanoparticles for combined tumor optical imaging and multiple phototherapies. *Theranostics* **2016**, *6* (13), 2367−2379.
(29) Zhou, Z.; Wang, Y.; Yan, Y.; Zhang, Q.; Cheng, Y. Dendrimer-templated ultrasmall and multifunctional photothermal agents for efficient tumor ablation. *ACS Nano* **2016**, *10* (4), 4863−4872.
(30) Song, G.; Wang, Q.; Wang, Y.; Lv, G.; Li, C.; Zou, R.; Chen, Z.; Qin, Z.; Huo, K.; Hu, R.; Hu, J. A low-toxic multifunctional nanoplatform based on Cu_9S_5@mSiO_2 core-shell nanocomposites: combining photothermal- and chemotherapies with infrared thermal imaging for cancer treatment. *Adv. Funct. Mater.* **2013**, *23* (35), 4281−4292.
(31) Huang, X.; Elsayed, I.; Qian, W.; Elsayed, M. Cancer cell imaging and photothermal therapy in the near-infrared region by using gold nanorods. *J. Am. Chem. Soc.* **2006**, *128* (6), 2115−2120.
(32) Li, T.; Li, C.; Ruan, Z.; Xu, P.; Yang, X.; Yuan, P.; Wang, Q.; Yan, L. Polypeptide-conjugated second near-infrared organic fluorophore for image guided photothermal therapy. *ACS Nano* **2019**, *13* (3), 3691−3702.
(33) Liu, B.; Li, C. X.; Chen, G. Y.; Liu, B.; Deng, X. R.; Wei, Y.; Xia, J.; Xing, B. G.; Ma, P. A.; Lin, J. Synthesis and optimization of MoS_2@Fe_3O_4-ICG/Pt(IV) nanoflowers for MR/IR/PA bioimaging and combined PTT/PDT/chemotherapy triggered by 808 nm laser. *Adv. Sci.* **2017**, *4* (8), 1600540.
(34) Wang, X. H.; Peng, H. S.; Yang, W.; Ren, Z. D.; Liu, X. M.; Liu, Y. A. Indocyanine green-platinum porphyrins integrated conjugated polymer hybrid nanoparticles for near-infrared-triggered photothermal and two-photon photodynamic therapy. *J. Mater. Chem. B* **2017**, *5* (9), 1856−1862.
(35) Li, X. S.; Peng, X. H.; Zheng, B. D.; Tang, J. L.; Zhao, Y. Y.; Zheng, B. Y.; Ke, M. R.; Huang, J. D. New application of phthalocyanine molecules: from photodynamic therapy to photothermal therapy by means of structural regulation rather than formation of aggregates. *Chem. Sci.* **2018**, *9* (8), 2098−2104.
(36) Zhang, Y.; He, L.; Wu, J.; Wang, K.; Wang, J.; Dai, W.; Yuan, A.; Wu, J.; Hu, Y. Switchable PDT for reducing skin photosensitization by a NIR dye inducing self-assembled and photodisassembled nanoparticles. *Biomaterials* **2016**, *107*, 23−32.
(37) Hu, W.; Ma, H.; Hou, B.; Zhao, H.; Ji, Y.; Jiang, R.; Hu, X.; Lu, X.; Zhang, L.; Tang, Y.; Fan, Q.; Huang, W. Engineering lysosome-targeting BODIPY nanoparticles for photoacoustic imaging and photodynamic therapy under near-infrared light. *ACS Appl. Mater. Interfaces* **2016**, *8* (12), 12039−12047.
(38) Ji, M.; Xu, M.; Zhang, W.; Yang, Z.; Huang, L.; Liu, J.; Zhang, Y.; Gu, L.; Yu, Y.; Hao, W.; An, P.; Zheng, L.; Zhu, H.; Zhang, J. Structurally well-defined Au@Cu_2-xS core-shell nanocrystals for improved cancer treatment based on enhanced photothermal efficiency. *Adv. Mater.* **2016**, *28* (16), 3094−3101.
(39) Geist, F.; Jackel, A.; Winter, R. F. Ligand based dual fluorescence and phosphorescence emission from BODIPY platinum complexes and its application to ratiometric singlet oxygen detection. *Inorg. Chem.* **2015**, *54* (22), 10946−10957.
(40) Zhang, G.; Musgrave, C. B. Comparison of DFT methods for molecular orbital eigenvalue calculations. *J. Phys. Chem. A* **2007**, *111* (8), 1554−1561.
(41) Li, G.; Hu, W. B.; Zhao, M. L.; Zhao, W. L.; Li, F. Y.; Liu, S. J.; Huang, W.; Zhao, Q. Rational design of near-infrared platinum(II)-acetylide conjugated polymers for photoacoustic imaging-guided synergistic phototherapy under 808 nm irradiation. *J. Mater. Chem. B* **2020**, *8* (33), 7356−7364.
(42) Song, X.; Chen, Q.; Liu, Z. Recent advances in the development of organic photothermal nano-agents. *Nano Res.* **2015**, *8* (2), 340−354.
(43) Wen, S.; Miao, X.; Fan, G.; Xu, T.; Jiang, L.; Wu, P.; Cai, C.; Zhu, J. Aptamer-conjugated Au nanocage/SiO_2 core-shell bifunctional nanoprobes with high stability and biocompatibility for cellular SERS imaging and near-infrared photothermal therapy. *ACS Sens.* **2019**, *4* (2), 301−308.
(44) Hu, J.; Liu, M.; Chen, Y.; Gao, F.; Peng, S.; Xie, B.; Li, C.; Zeng, X.; Zhang, X. Immobilized liquid metal nanoparticles with improved stability and photothermal performance for combinational therapy of tumor. *Biomaterials* **2019**, *207*, 76−88.
(45) Jang, B.; Park, J.; Tung, C.; Kim, I.; Choi, Y. Gold nanorod-photosensitizer complex for near-infrared fluorescence imaging and photodynamic/photothermal therapy in vivo. *ACS Nano* **2011**, *5* (2), 1086−1094.
(46) Zheng, M.; Zhao, P.; Luo, Z.; Gong, P.; Zheng, C.; Zhang, P.; Yue, C.; Gao, D.; Ma, Y.; Cai, L. Robust ICG theranostic nanoparticles for folate targeted cancer imaging and highly effective photothermal therapy. *ACS Appl. Mater. Interfaces* **2014**, *6* (9), 6709−6716.
(47) Song, X.; Liang, C.; Gong, H.; Chen, Q.; Wang, C.; Liu, Z. Photosensitizer-conjugated albumin-polypyrrole nanoparticles for imaging-guided in vivo photodynamic/photothermal therapy. *Small* **2015**, *11* (32), 3932−3941.
(48) Hu, K.; Xie, L.; Zhang, Y. D.; Hanyu, M.; Yang, Z. M.; Nagatsu, K.; Suzuki, H.; Ouyang, J.; Ji, X. Y.; Wei, J. J.; Xu, H.; Farokhzad, O. C.; Liang, S. H.; Wang, L.; Tao, W.; Zhang, M. R. Marriage of black phosphorus and Cu^{2+} as effective photothermal agents for PET-guided combination cancer therapy. *Nat. Commun.* **2020**, *11*, 2778 DOI: 10.1038/s41467-020-16513-0.

https://dx.doi.org/10.1021/acs.inorgchem.0c02631
Inorg. Chem. XXXX, XXX, XXX−XXX